

Short Communication

## Effects of Carbon Additives on the HRPSoC Performance of Lead Carbon Batteries and Their Low Temperature Performance

Yi Jiang<sup>1</sup>, Hao Zhu<sup>2</sup>, Chunlai Yu<sup>3</sup>, Xu Cao<sup>1</sup>, Lin Cheng<sup>1</sup>, Ruhong Li<sup>2</sup>,  
Shaoqiang Yang<sup>2</sup>, Changsong Dai<sup>2,\*</sup>

<sup>1</sup> Wuhan NARI Limited Company of State Grid Electric Power Research Institute, 430074 Wuhan, China

<sup>2</sup> MIIT Key Laboratory of Critical Materials Technology for New Energy Conversion and Storage, School of Chemistry and Chemical Engineering, Harbin Institute of Technology, 150001 Harbin, China

<sup>3</sup> Heilongjiang Electric Power Research Institute, 150001 Harbin, China

\*E-mail: [changsd@hit.edu.cn](mailto:changsd@hit.edu.cn)

Received: 26 June 2017 / Accepted: 22 September 2017 / Published: 12 October 2017

---

Effects of different special carbon materials on the performance of negative plates were studied. The addition of carbon materials P1 and P2 greatly improved the high-rate partial-state-of-charge (HRPSoC) cycle performance of the batteries. A negative plate completed 18489 HRPSoC micro-cycles in the first cycle-set when the concentration of P2 was 0.9%. Special properties are required for the carbon materials to be used as additives to the negative electrode materials. Firstly, the carbon material added to the negative electrode should have a good binding force with lead and lead sulfate. Secondly, the carbon material should have a large specific surface area and a larger pore volume. Addition of bismuth sulfide can inhibit the hydrogen evolution of the lead-carbon negative plates. Negative electrodes modified with a C/Bi<sub>2</sub>S<sub>3</sub> composite exhibited good low temperature performance.

---

**Keywords:** carbon materials, negative electrode modification, HRPSoC, hydrogen evolution behavior, low temperature performance

### 1. INTRODUCTION

It is a good idea to install a start/stop power supply in a car to alleviate the pressure of energy crisis and environmental pollution, Traditional lead-acid batteries have been used for this purpose because of their low price and good rate performance. [1, 2]. However, because of their low energy density, the negative plates are prone to sulfate attack when circulated under high-rate partial-state-of-

charge (HRPSoC) [3-6], which makes it difficult for negative plates to accept regenerative currents and to provide the power to start the engine or for acceleration. This drawback has limited the further application of traditional lead-acid batteries for this purpose. Nakamura et al. found that the addition of the appropriate species and content of carbon materials to a negative electrode plate could inhibit the irreversible sulfation of the negative plate at HRPSoC, thereby increasing the battery's cycle life [7, 8]. The improved lead-acid batteries are called as lead-carbon battery [9, 10].

The good electrical conductivity, capacitance characteristics and high specific surface areas of carbon materials can enhance the utilization of the negative electrode active materials and the dispersibility of the negative active materials, thereby suppressing the crystallization or deactivation of the lead sulfate crystals [11-13]. In addition, the carbon materials can also provide a double-layer capacitor under high-power charge and discharge cycling, buffering and reducing the damage to the negative electrode by the large current used to facilitate the circulation of the negative electrode under HRPSoC conditions [14-17]. As a carbon material can be added directly to a negative electrode, lead-carbon batteries can be manufactured in a traditional lead-acid battery production workshop, which makes large-scale production and application of lead-carbon batteries possible [18-20]. However, special properties are required for a carbon material to be used as an additive to inhibit the irreversible sulfation of a negative plate in the HRPSoC and the material selection process can be complex [21-23]. D. Pavlov et al. [24, 25] added seven types of carbon black materials (PR1, PR2, PR3, PR4, AC2, AC3, AC4) and one activated carbon material (AC1) to the negative electrode plates to study the effects of those materials on the performance of lead carbon batteries under HRPSoC cycling. They found that the battery with 0.5% of AC2 carbon black had the longest cycling life, which was about 22000 times. Ebner et al. [26] found that the surface morphology, porosity, particle size, conductivity, impurity content, and degree of ordering of carbon black all had influence on the cycle life of batteries.

Carbon materials have low hydrogen evolution potentials, which may cause a higher degree of hydrogen evolution for lead-acid batteries if carbon materials are used as additives to a negative plate. Hydrogen evolution not only can result in serious loss in electrolytes during cycling, but also can affect adversely the charging efficiency of a battery and can destroy the structure of a negative plate. It can also cause a negative plate internal resistance to increase. Eventually the performance of a battery will attenuate more quickly because of hydrogen evolution [27]. At present, there are few studies on the methods of suppressing the hydrogen evolution of lead-carbon batteries. LT Lam et al. [28] studied the effect of 17 elements on the hydrogen evolution and oxygen evolution of lead-acid batteries. They found that nickel and selenium significantly increased the hydrogen evolution of lead-carbon batteries while bismuth, silver, calcium, cadmium and zinc inhibited hydrogen evolution and a mixture of bismuth, zinc and silver could suppress hydrogen precipitation the most. Lang et al [29, 30] used two ways to suppress the negative hydrogen of lead-carbon batteries. In the first method, 0.6% of an indium oxide, cerium oxide, barium stearate and gallium oxide mixture was added to a negative lead paste, in the second method, lead sulfate was deposited on a carbon material. It was found that the addition of a mixture of indium oxide and gallium oxide and the deposition of lead sulfate on a carbon material could both inhibit the hydrogen precipitation very well [31].

The present study has focused on research on the idea of carbon material selection processes and on the inhibition of hydrogen deposition, especially at a low temperature. Different carbon

materials P1 and P2 were added into negative active materials to form negative plates. The working state of a lead-carbon battery in a hybrid electric vehicle (HEV) was simulated and appropriate contents and types of carbon materials were screened. Based on the results obtained from the above experiments, hydrogen evolution behavior of negative electrodes for lead-carbon batteries was studied. Using the optimal conditions obtained, a modified negative electrode plate was constructed and its low temperature performance was evaluated.

## 2. EXPERIMENTAL

### 2.1. Preparation of C/Bi<sub>2</sub>S<sub>3</sub> composites

Mesoporous carbon materials P1 and P2 were purchased from Aladdin. C/Bi<sub>2</sub>S<sub>3</sub> composites were synthesized by using a hydrothermal method. Bi(NO<sub>3</sub>)<sub>3</sub> of 1.2 g and 10 mol of ethylene glycol were mixed and stirred for 10 min. Then 0.6 g of P2 and 20 ml of distilled water were added into the above mixture and stirred for 20 min. This mixture was then filtered and rinsed with ethyl alcohol and distilled water. The obtained carbon material was added into 10 ml of distilled water, which was labelled as mixture A. Na<sub>2</sub>S of 1.2 g was dissolved in 10ml of distilled water, which was marked as mixture B. The mixture B was added dropwise to the mixture A and stirred rapidly to prepare a black precursor. Subsequently, 1.0 g of Co(NH<sub>2</sub>)<sub>2</sub> was added to this precursor. The final mixture was then transferred to an 80 ml Teflon-lined stainless steel autoclave and kept at 60 °C for 12 h. The powder was filtered and rinsed with deionized water and ethanol several times, and dried at 60 °C for 12 h.

### 2.2. Physical Characterizations

X-ray diffraction (Panalytical, X'PERT PRO MPD) using Cu K $\alpha$  radiation ( $\lambda = 0.15406$  nm) was employed to characterize the crystal phase of the sample. Scanning electron microscopy (FEI, Helios Nanolab 600i) was conducted to characterize the particle shape and size. Raman spectra (Renishaw, InVia) were recorded to evaluate the molecular vibrations, rotations and molecular structures of the material. The Brunauer–Emmett–Teller (BET) (Micromeritics, ASAP2020) test was used to obtain the specific surface area, the pore volume and the pore size distribution of the material.

### 2.3. Preparation of the negative electrodes and unit cell

The negative electrode sheets were prepared using lead oxide power, acetylene black, short carbon fibers, barium sulfate, humic acids, H<sub>2</sub>SO<sub>4</sub> (1.28 g cm<sup>3</sup>), and different amounts of each carbon type. The degree of oxidation of lead oxide was 76 %. The contents of acetylene black, barium sulfate, humic acids and short carbon fibers were 0.2 wt %, 0.6 wt %, 0.16 wt % and 0.05 wt % (versus the lead oxide), respectively. The amount of acetylene black was varied from 0 % to 1.0 wt %, and the content of CB was 0.2 wt %, 0.5 wt %, and 1.0 wt %. The preparation method of the negative electrode sheets was as follows: First, a certain amount of lead oxide and carbon additives were ground using an agate

mortar for a few minutes; then, other negative additives were added to the agate mortar and ground in turn. Short fibers uniformly dispersed by deionized water were added to the mortar and stirred for a few minutes. Finally, a certain amount of  $\text{H}_2\text{SO}_4$  was added to the mixture dropwise, and deionized water was used to adjust the consistency of the lead paste. A certain amount of lead paste was coated on a Pb-Ca grid with a geometric area of  $112 \times 680 \text{ mm}^2$  to prepare the negative electrode sheets. All the as-prepared negative electrode sheets were cured under carefully controlled conditions at  $35 \text{ }^\circ\text{C}$  for 2 hours and  $65 \text{ }^\circ\text{C}$  for 4 hours at a proper humidity level. In the spiral lead carbon battery assembly, the cast plate was used as the negative current collector and lead foil is used as the positive current collector. The batteries were formed in  $\text{H}_2\text{SO}_4$  solution ( $1.05 \text{ g cm}^3$ ) with a current of  $2.8 \text{ A/g}$  with a commercial formation procedure.

#### 2.4. Electrochemical measurements

The galvanostatic charge-discharge tests at different temperatures were conducted on a battery test system (Neware, China) at  $0.1 \text{ C}$ . The hydrogen evolution behaviors of the as-prepared materials were evaluated using a three-electrode system. Linear sweep voltammetry was performed with a scanning rate of  $5 \text{ mV s}^{-1}$  in a range from  $0 \text{ V}$  to  $-1.5 \text{ V}$  (vs.  $\text{Hg/Hg}_2\text{SO}_4$ ).

### 3. RESULTS AND DISCUSSION

#### 3.1. Filtration of carbon materials

Adding a certain amount of carbon in the negative electrode is a potential route to relieve the extent of sulfate accumulation and improve the cycle-life of batteries in HRPSoC duty. The specific physical properties of the carbon material tend to affect the final effect [15]. Xiang et al. [32] reported that adding activated carbon with a particle size range of tens of microns to the NAM could notably prolonge the HRPSoC cycle life, whereas the cycle numbers were much lower for a battery that incorporated carbon particles with a much smaller size (several microns) or one without activated carbon. Most researchers have improved the performance of the battery by using carbon black with relatively small specific surface area (SSA) as an additive, and have achieved good results. Ellen et al [21] selected different carbon blacks with a SSA about  $240 \text{ m}^2 \text{ g}^{-1}$  as additives and added with quantities of between 0.2% and 2% to the negative active material. They found that batteries with carbons in the negative active masses displayed drastically decreased sulfation in the negative plate. We selected two carbon black material P1 and P2 with high specific surface area to study whether adding a small amount of these carbon black materials could achieve the same effect or not. Fig. 1 presents the SEM images of carbon materials P1 and P2. The SEM images evidence that both types of carbon materials had flaky structures with rough surfaces. The size of P1 was larger than that of P2. The specific surface area and pore size distribution of carbon materials were characterized by the  $\text{N}_2$  adsorption desorption method. The results are shown in Table 1 and Fig. 2. The carbon material P1 had a smaller specific surface area, a larger pore volume, and a larger pore size than P2. Both the carbon materials P1 and P2 had mesoporous structures according to their pore size distribution.

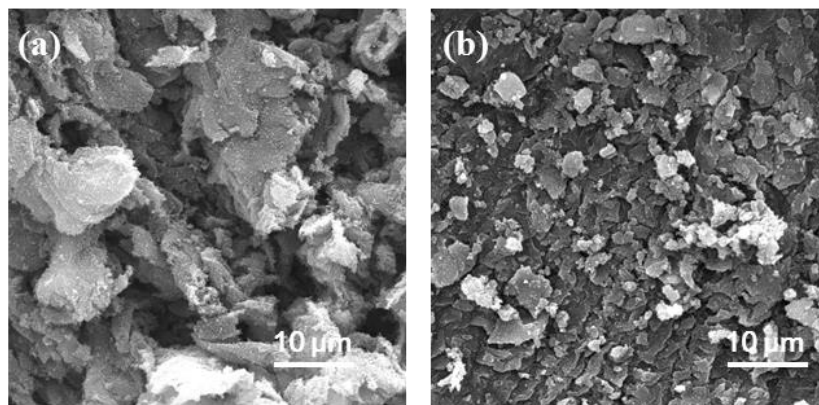


**Figure 1.** SEM images of carbon materials: a) P1 and b) P2

**Table 1.** The specific surface area, average pore volume and average pore size of carbon materials

Types	Specific surface area (m <sup>2</sup> /g)	Average pore volume (cm <sup>3</sup> /g)	Average pore size (nm)
P1	379.08	2.26	29.19
P2	1390.07	1.32	8.32

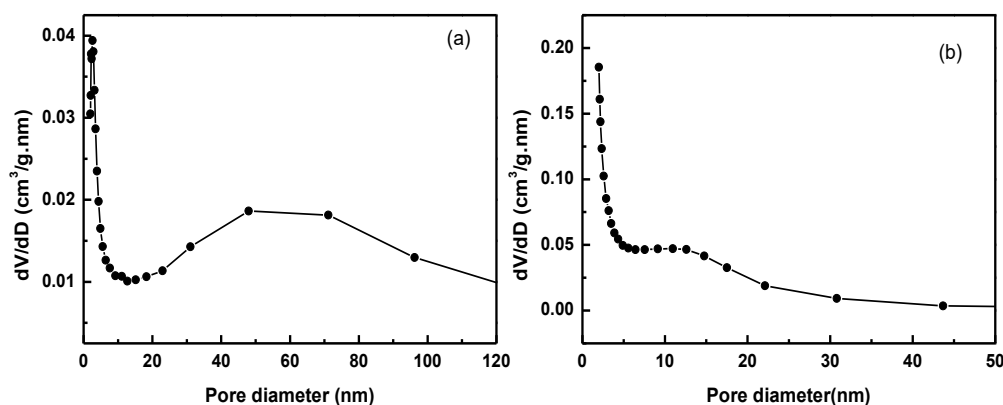


**Figure 2.** The pore size distribution of carbon materials: a) P1 and b) P2

The Raman spectra for carbon materials (Figure 3) exhibit two peaks located at 1580 cm<sup>-1</sup> and 1360 cm<sup>-1</sup>, respectively. The peak at 1580 cm<sup>-1</sup> is the G-band, which corresponds to the stretching motion of all sp<sup>2</sup> atoms in the carbon ring or carbon long chain of carbon material. The peak at 1360 cm<sup>-1</sup> is the D-band, which is induced by defects and disorder in the lattice of carbon atoms. The disorder degree of carbon material (R) is the ratio of peak intensity of the D-band ( $I_D$ ) to the G-band ( $I_G$ ). For the carbon materials P1 and P2, the peak intensities of the D-band are close to that of the G-band. This result means that their disorder degree R was close to 1, indicating that the carbon materials P1 and P2 are highly disordered. The disorder degree of P1 was greater than that of P2, demonstrating that the proportion of amorphous carbon in P1 was higher than that in P2.

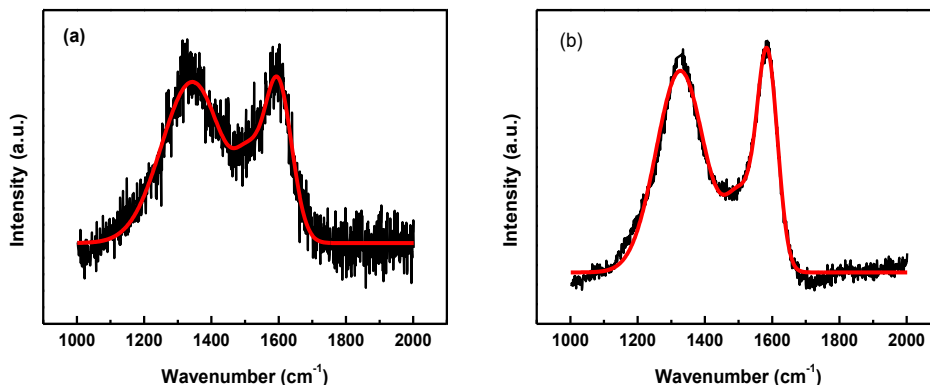


**Figure 3.** Raman spectra of carbon materials: a) P1; b) P2

3.2. Influence of carbon materials on the HRPSoC performance

**Table 2.** HRPSoC cycle life of cells at 2 C charge and discharge rate

	1 <sup>st</sup> HRPSoC cycle times	2 <sup>nd</sup> HRPSoC cycle times
Commercial	2060	0
Without Carbon material	950	1545
0.9% P1	15491	15857
0.9% P2	18489	17882

The results of cycle test under HRPSoC are shown in Table 2 and Fig 4. As seen in Table 2, the first cycle test under HRPSoC was 2060 times for a commercial battery, but the second cycle test was 0 time because the discharge voltage was too low. The first cycle with HRPSoC was 950 times and the second HRPSoC cycle was 1545 times for the negative plate without addition of carbon material. The cycle performance of a battery under HRPSoC was greatly improved when the carbon material P1 or P2 was added to the negative plate. The first two cycle numbers of a HRPSoC battery with P1 were 15491 and 15857 times, and the first two cycle numbers of a HRPSoC battery with P2 were 18489 and 17882 times. Compared with the first HRPSoC cycle, the second cycle of the batteries with the carbon material P1 or P2 additives were not attenuated.

After the cycle test, the negative plates were charged at a current of 0.1 C. The surface and internal morphology of the negative plates were observed by SEM and the images are presented in Fig.5. The commercial negative plate had a more compact surface after 2000 cycles and it showed a loose internal structure. For the negative plate with 0.9 wt. % P1, many large crystals appeared on the surface and in the internal structure of the plate after 32000 cycles. The large crystals were composed of lead sulfate. For the negative plate with 0.9 wt. % P2 after 36000 cycles, the negative active material was composed of smaller particles which were interconnected in a loose structure.

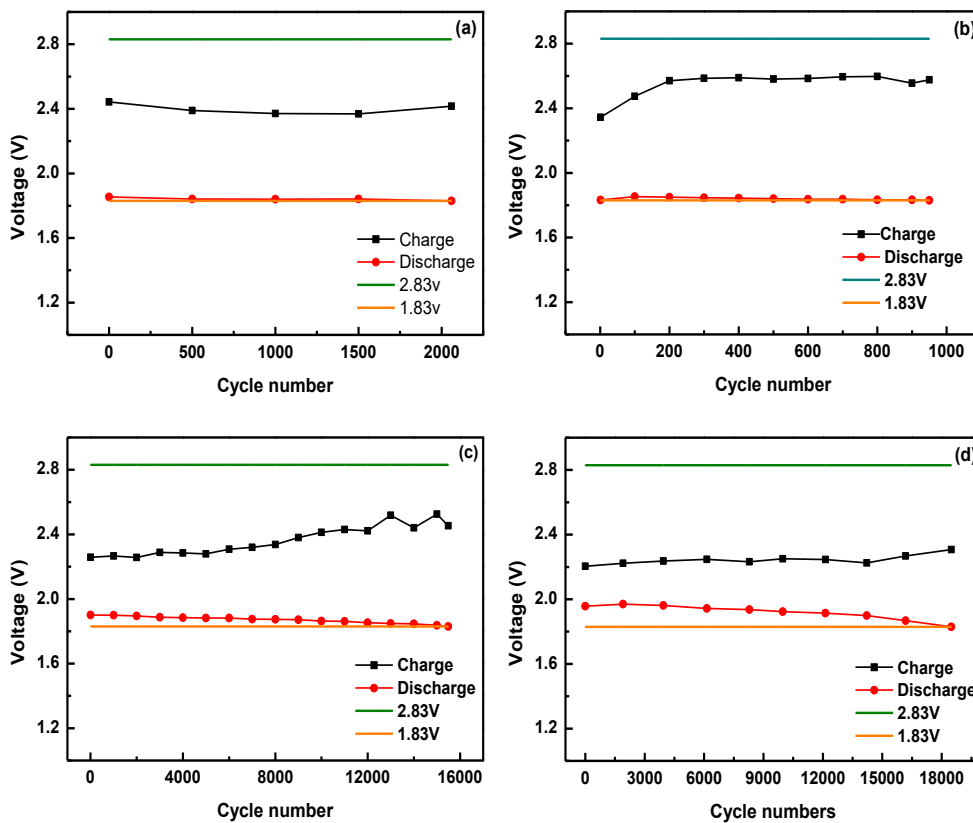


**Figure 4.** Changes of the  $V_{\text{charge}}$  and  $V_{\text{discharge}}$  as a function of cycle number under HRPSoC conditions for the simulated batteries: a) commercial; b) 0 wt. % carbon; c) 0.9 wt. % P1 and d) 0.9 wt. % P2

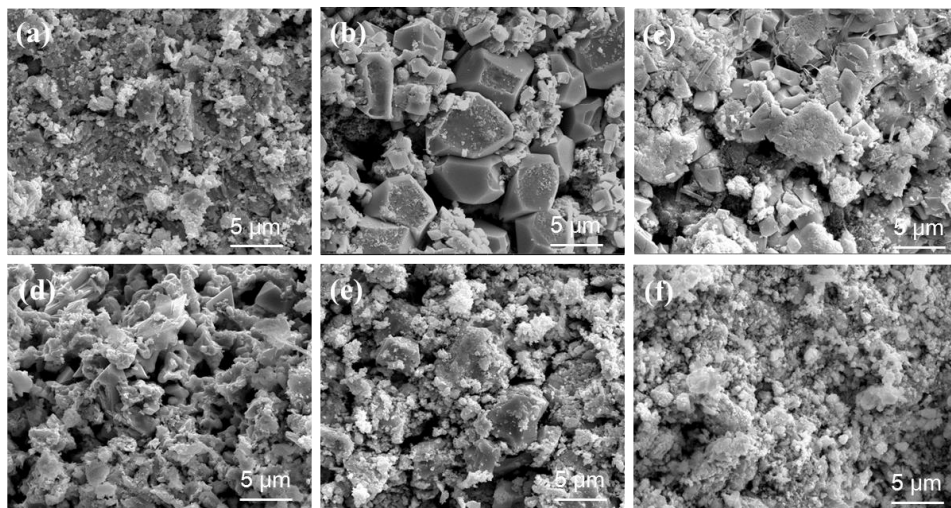


**Figure 5.** Microstructures of NAM with different carbon materials after the cycle test: a) commercial battery, surface; b) commercial battery, interior; c) 0.9 wt. % P1, surface; d) 0.9 wt. % P1, interior; e) 0.9 wt. % P2, surface and f) 0.9 wt. % P2, interior

**Table 3.** EDS results of negative plates after cycle test

element	commercial, surface	commercial, internal	0.9 wt. % P1, surface	0.9 wt. % P1, internal	0.9 wt. % P2, surface	0.9 wt. % P2, internal
C	8.09	20.68	11.09	13.10	9.91	13.02
O	16.24	12.24	18.85	13.23	18.43	18.05
S	3.46	1.64	4.37	1.55	3.32	1.68
Pb	72.21	65.44	65.69	72.13	68.33	67.25

As shown in Table 3, the sulfur content on the surface of each of the fully charged negative plate was greater than that in its internal structure. In the long-term high current discharge process, denser lead sulfate was produced on the surface of the negative plate, which prevented the hydrogen sulfate ions and the electrolyte from entering into the internal structure of the negative electrode plate, resulting in less lead sulfate generated inside the negative plate. The surface and the internal sulfur contents of the commercial negative plate were as high as 3.46 % and 1.64 %, respectively, just after 2060 cycles. For the negative plate with 0.9 wt. % P1, the similar sulfur content appeared on the surface and in the internal structure of plate after 31348 cycles, which were 15 times more than that for the commercial battery. It can be inferred that the addition of the carbon material P1 can retard the irreversible sulfation of the negative plate. Similarly, the addition of the carbon material P2 could also delay irreversible sulfation of the negative plate based on the surface and the internal sulfur contents of 3.22 % and 1.68 %, respectively, after 36371 cycles. The effect of these carbon materials on the HRPSoC cycle performance of a battery was a result of certain properties of carbon materials. First, these carbon materials could bind lead/lead sulphate well. Because of its larger specific surface area, the carbon material P2 could provide more reaction sites, leading to the conversion of lead sulfate to lead. Therefore, the sulfation of the negative plate could be alleviated, which can explain that the HRPSoC cycle performance of P2 was slightly better than that of P1. Fernandez et al. [6, 33] also reported that the addition of medium/high SSA carbon to NAM affected the performance of the negative plates. A higher SSA enhances electrochemically active surface, decreases electrode polarization, thus improving the cycle performance of negative plates. However, other material characteristics should not be ignored, because synergistic effects may be possible. Further studies should attend more closely to the influence of carbons containing different pores, average particle sizes, as well as conductivities on the cycle performance.

### 3.3. Study on hydrogen evolution behavior of negative electrode

The addition of carbon materials tended to accelerate the exchange of hydrogen on the negative plate. The addition of Bismuth sulfide in the 0.9 wt. % P2 plate was further studied. Typical X-ray diffractions (XRD) pattern of the as-fabricated C/Bi<sub>2</sub>S<sub>3</sub> composite is displayed in Fig. 6a. All of the diffraction peaks can be assigned to the orthorhombic Bi<sub>2</sub>S<sub>3</sub> (S.G. Pbnm) with the lattice parameters a-11.149 Å, b-11.304 Å and c-3.981 Å, which are in good agreement with the JCPDS card No. 17-0320. No miscellaneous peaks can be observed in the XRD pattern, indicating that the C/Bi<sub>2</sub>S<sub>3</sub> composite

material was successfully synthesized by the hydrothermal method. As can be seen from Fig. 6b, the morphology of C/Bi<sub>2</sub>S<sub>3</sub> composite material was substantially the same as that of the carbon material P2. It is clear that the Bi<sub>2</sub>S<sub>3</sub> nanotubes are well combined with the carbon material P2, which are indicative of no obvious influence of Bi<sub>2</sub>S<sub>3</sub> modification on original morphology. The in-situ form of C/Bi<sub>2</sub>S<sub>3</sub> composite benefit the good contact and robust binding of AC and Bi<sub>2</sub>S<sub>3</sub> a lot.

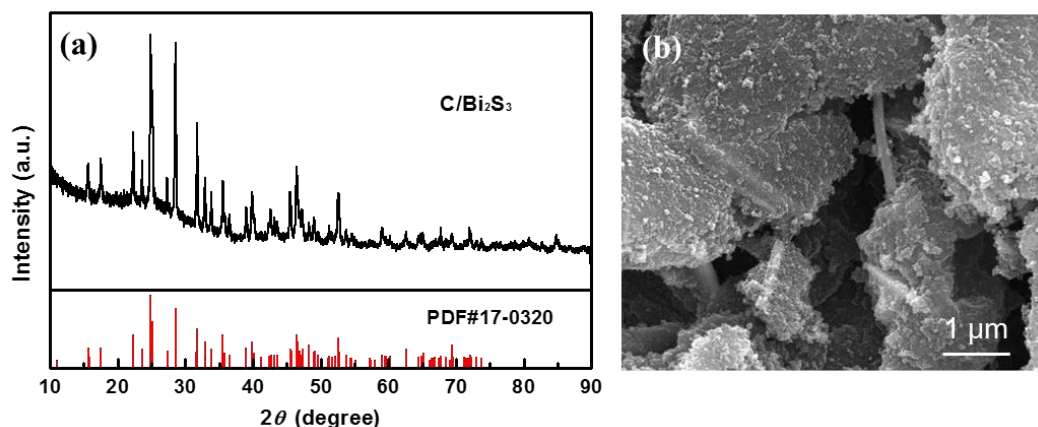


Figure 6. XRD pattern (a) and SEM image (b) of C/Bi<sub>2</sub>S<sub>3</sub> composite

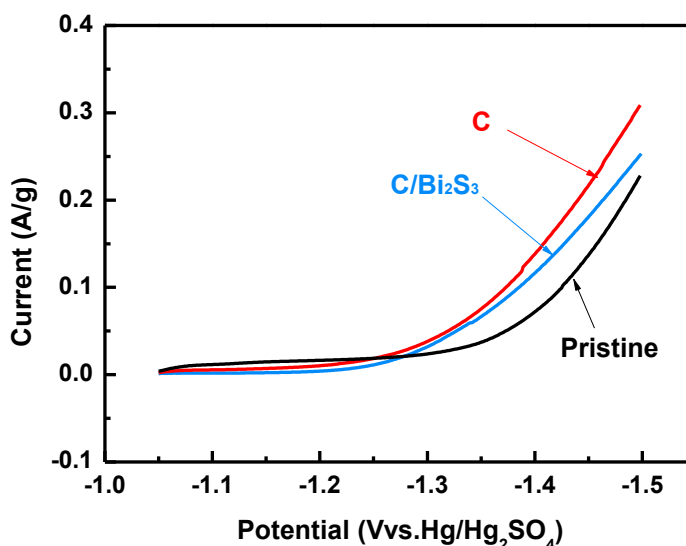


Figure 7. The linear potential scanning curves of different negative electrodes

Fig. 7 shows the linear sweep voltammetry of the three types of negative electrodes. It can be seen that the hydrogen evolution potentials of the negative plates with C or C/Bi<sub>2</sub>S<sub>3</sub> were significantly reduced due to the low hydrogen evolution over-potential of carbon, which was consistent with the previous reports. It is worth noting that the hydrogen evolution rate of the negative electrode with the C/Bi<sub>2</sub>S<sub>3</sub> composite material was lower than that of the electrode with

pure carbon, indicating that the C/Bi<sub>2</sub>S<sub>3</sub> composite could reduce the hydrogen evolution rate of a negative electrode. The HER potential of C/Bi<sub>2</sub>S<sub>3</sub> composite electrode was obviously negative shifted (~-1.23 V). Noticeably, AC modified with 4 wt. % Bi<sub>2</sub>O<sub>3</sub> can also suppress the hydrogen evolution by negatively shifting the HER onset potential to -1.12 V, which agrees well with the previously reports [27]. Obviously, C/Bi<sub>2</sub>S<sub>3</sub> is more effective in inhibiting HER compared to AC/Bi<sub>2</sub>O<sub>3</sub> in terms of negatively shifted potential. The excellent behavior of C/Bi<sub>2</sub>S<sub>3</sub> composites is likely originated from the more uniform distribution and stronger interaction between C and Bi<sub>2</sub>S<sub>3</sub>.

### 3.4. Low temperature performance of spiral battery

The electrochemical performance of a spiral lead carbon battery (12 V, 20 Ah) with a negative plate modified with C/Bi<sub>2</sub>S<sub>3</sub> was tested at various temperatures, as shown in Fig.8. At 0.1 C, the spiral lead carbon battery delivered capacities of 19.1, 11.7 and 0.6 Ah at 0, -25 and -40 °C, respectively, corresponding to capacity retention ratio of 89.7 %, 54.9 % and 2.9 % measured at 25 °C (21.3 Ah). At lower temperatures, the plateaus were shorter and the potential differences between the charge and discharge plateaus were smaller. The columbic efficiency was close to 100 % at all the temperatures.

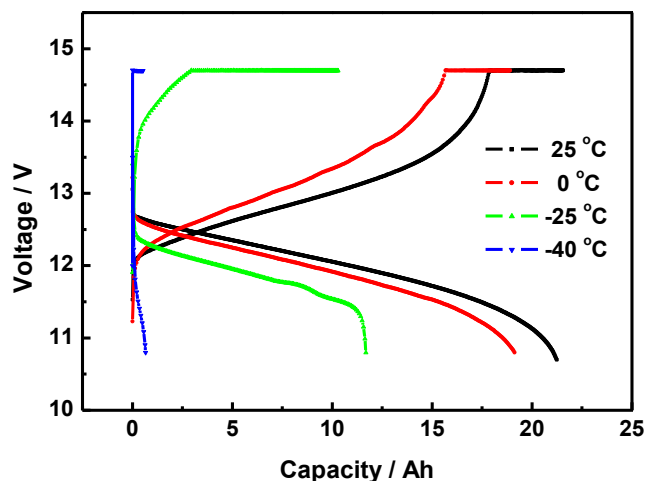


Figure 8. The low temperature performance of a spiral lead carbon battery

## 4. CONCLUSION

The effects of carbon materials P1 and P2 on the electrochemical performance under HRPSoC condition were studied. It was found that the addition of carbon materials P1 and P2 could significantly improve the HRPSoC cycle performance. When 2% P2 was added to a negative plate, the battery completed 18489 HRPSoC micro-cycles in the first cycle and 17882 HRPSoC micro-cycles in the second cycle. The effect of carbon material on the HRPSoC performance of the negative electrode was a result of various properties of the carbon materials. The excellent adhesion between the carbon

material and the lead and/or lead sulfate was critical; a larger specific surface area and a larger pore volume were also important. In addition, the conductivity and other characteristics of the carbon materials also affected the HRPSOC cycle performance. However, the addition of carbon did aggravate the hydrogen evolution rate of the electrode. C/Bi<sub>2</sub>S<sub>3</sub> composite material can reduce the hydrogen evolution rate of the negative electrode. The prepared electrode modified with C/Bi<sub>2</sub>S<sub>3</sub> composite exhibited good low temperature performance.

## References

1. B. Scrosati, J. Garche, *J Power Sources*, 195 (2010) 2419-2430.
2. C. Liu, F. Li, L.P. Ma, H.M. Cheng, *Adv Mater*, 22 (2010) E28-E62.
3. D.P. Boden, D.V. Loosemore, M.A. Spence, T.D. Wojcinski, *J Power Sources*, 195 (2010) 4470-4493.
4. L.T. Lam, N.P. Haigh, C.G. Phyland, A.J. Urban, *J Power Sources*, 133 (2004) 126-134.
5. H. Yang, Y. Qiu, X. Guo, *Electrochim Acta*, 235 (2017) 409-421.
6. X. Zou, Z. Kang, D. Shu, Y. Liao, Y. Gong, C. He, J. Hao, Y. Zhong, *Electrochim Acta*, 151 (2015) 89-98.
7. X.S. Lang, D.L. Wang, C.Y. Hu, S.Z. Tang, J.S. Zhu, C.F. Guo, *J Power Sources*, 270 (2014) 9-13.
8. S. Atlung, B. Zachaustriansen, *J Power Sources*, 52 (1994) 201-209.
9. J. Furukawa, T. Takada, D. Monma, L.T. Lam, *J Power Sources*, 195 (2010) 1241-1245.
10. L.T. Lam, R. Louey, *J Power Sources*, 158 (2006) 1140-1148.
11. Y. Shi, C.A. Ferone, C.D. Rahn, *J Power Sources*, 221 (2013) 177-185.
12. R. Marom, B. Ziv, A. Banerjee, B. Cahana, S. Luski, D. Aurbach, *J Power Sources*, 296 (2015) 78-85.
13. P.T. Moseley, D.A.J. Rand, K. Peters, *J Power Sources*, 295 (2015) 268-274.
14. K. Dhanabalan, T. Sadhasivam, S.C. Kim, J.J. Eun, J. Shim, D. Jeon, S.-H. Roh, H.-Y. Jung, *J Mater Sci-Mater El*, 28 (2017) 10349-10356.
15. Q. Long, G. Ma, Q. Xu, C. Ma, J. Nan, A. Li, H. Chen, *J Power Sources*, 343 (2017) 188-196.
16. P. Tong, R. Zhao, R. Zhang, F. Yi, G. Shi, A. Li, H. Chen, *J Power Sources*, 286 (2015) 91-102.
17. H. Yang, Y. Qiu, X. Guo, *Electrochim Acta*, 215 (2016) 346-356.
18. L.Y. Wang, W.F. Zhang, L. Gu, Y. Gong, G.P.P. Cao, H.L. Zhao, Y.S. Yang, H. Zhang, *Electrochim Acta*, 222 (2016) 376-384.
19. S. Logeshkumar, R. Manoharan, *Electrochim Acta*, 144 (2014) 147-153.
20. X. Li, Y. Zhang, Z. Su, Y. Zhao, X. Zhao, R. Wang, *J Appl Electrochem*, 47 (2017) 619-630.
21. E. Ebner, D. Burow, A. Börger, M. Wark, P. Atanassova, J. Valenciano, *J Power Sources*, 239 (2013) 483-489.
22. E. Ebner, D. Burow, J. Panke, A. Börger, A. Feldhoff, P. Atanassova, J. Valenciano, M. Wark, E. Rühl, *J Power Sources*, 222 (2013) 554-560.
23. J. Settelein, H. Lorrman, G. SEXTL, *Electrochim Acta*, 233 (2017) 173-180.
24. D. Pavlov, T. Rogachev, P. Nikolov, G. Petkova, *J Power Sources*, 191 (2009) 58-75.
25. D. Pavlov, P. Nikolov, T. Rogachev, *J Power Sources*, 196 (2011) 5155-5167.
26. E. Ebner, D. Burow, J. Panke, A. Borger, A. Feldhoff, P. Atanassova, J. Valenciano, M. Wark, E. Ruhl, *J Power Sources*, 222 (2013) 554-560.
27. J. Lian, W. Li, F. Wang, J. Yan, K. Wang, S. Cheng, K. Jiang, *J Electrochem Soc*, 164 (2017) A1726-A1730.
28. L.T. Lam, H. Ceylan, N.P. Haigh, T. Lwin, D.A.J. Rand, *J Power Sources*, 195 (2010) 4494-4512.
29. X.S. Lang, D.L. Wang, J.S. Zhu, *J Power Sources*, 272 (2014) 176-182.

30. X.S. Lang, D.L. Wang, S.Z. Tang, J.S. Zhu, C.F. Guo, *J Power Sources*, 271 (2014) 354-359.
31. L. Zhao, B.S. Chen, D.L. Wang, *J Power Sources*, 231 (2013) 34-38.
32. J. Xiang, P. Ding, H. Zhang, X. Wu, J. Chen, Y. Yang, *J Power Sources*, 241 (2013) 150-158.
33. M. Fernández, J. Valenciano, F. Trinidad, N. Muñoz, *J Power Sources*, 195 (2010) 4458-4469.

© 2017 The Authors. Published by ESG ([www.electrochemsci.org](http://www.electrochemsci.org)). This article is an open access article distributed under the terms and conditions of the Creative Commons Attribution license (<http://creativecommons.org/licenses/by/4.0/>).